1 .

IEEE Access
Multidisciplinary | Rapid Review | Open Access Journal

Date of publication 2 February 2023, date of current version 2 February 2023.

Digital Object Identifier 10.1109/ACCESS.2023.DOI

Viewing Bias Matters in 360° Videos Visual Saliency Prediction

PENG-WEN CHEN[1], TSUNG-SHAN YANG[2], GI-LUEN HUANG[3], CHIA-WEN HUANG[3], YU-CHIEH CHAO[4], CHIEN-HUNG LU[5], PEI-YUAN WU[6],

[1]Graduate Institute of Communication Engineering, National Taiwan University, 10617 Taipei, Taiwan (e-mail: domokun0413@gmail.com)
[2]Department of Electrical Engineering, University of Southern California (e-mail: tsungsha@usc.edu)
[3]Graduate Institute of Communication Engineering, National Taiwan University, 10617 Taipei, Taiwan (e-mail: r09942171@ntu.edu.tw, r11942157@ntu.edu.tw)
[4]Institute of Information Science, Academia Sinica, 11529 Taipei, Taiwan (e-mail: vpj870331@citi.sinica.edu.tw)
[5]Unusly, San Francisco, USA (e-mail: luke@unusly.com)
[6]Electrical Engineering, National Taiwan University, 10617 Taipei, Taiwan (e-mail: peiyuanwu@ntu.edu.tw)

Corresponding author: Pei-Yuan Wu (e-mail: peiyuanwu@ntu.edu.tw).

ABSTRACT 360° video has been applied to many areas such as immersive contents, virtual tours, and surveillance systems. Compared to the field of view prediction on planar videos, the explosive amount of information contained in the omni-directional view on the entire sphere poses an additional challenge in predicting high-salient regions in 360° videos. In this work, we propose a visual saliency prediction model that directly takes 360° video in the equirectangular format. Unlike previous works that often adopted recurrent neural network (RNN) architecture for the saliency detection task, in this work, we utilize 3D convolution to a spatial-temporal encoder and generalize SphereNet kernels to construct a spatial-temporal decoder. We further study the statistical properties of viewing biases present in 360° datasets across various video types, which provides us with insights into the design of a fusing mechanism that incorporates the predicted saliency map with the viewing bias in an adaptive manner. The proposed model yields state-of-the-art performance, as evidenced by empirical results over renowned 360° visual saliency datasets such as Salient360!, PVS, and Sport360.

INDEX TERMS Visual saliency prediction, 360° videos, viewing bias, deep learning.

I. INTRODUCTION

360° video, a new multimedia type, has become popular due to its immersive experiences [1]–[3]. Compared to conventional planar videos, 360° videos [4] capture omni-directional field of view in one frame. We can enjoy this immersive experience by drag-and-drop the mouse on social media platforms or changing our head and eye movements with head-mounted display devices. Consumer can even create a 360° video with an off-the-shelf 360° camera, such as Insta360, Samsung Gear360, or Ricoh Theta, and shared them on Facebook or YouTube.

The emerging of 360° videos shows that 360° videos will become a major video format in the near future. However, it's hard for users to explore a whole frame of 360° videos because users cannot observe the content outside the FoV associated with human eyes; users need to change the viewing angles regularly to see the whole 360° environment. To relieve the issue, methods of human visual saliency prediction that focused on modeling human visual attention and identifying users' interest in 360° videos are recently developed [5]–[8].

Nowadays, methods modeling 360° visual saliency (VS) prediction are still limited. Although there are dozens of VS prediction models available for planar videos [9]–[11], such models are not suitable to the 360° video which has its own characteristics that must be taken into consideration. First, 360° videos are generally presented in equirectangular projection format which oversamples points in polar regions. Second, in planar videos, a gaussian kernel center bias is usually added into the prediction since users tend to watch the center part of an image [12], [13]. However, since 360° videos capture the whole picture with no dead spots, the human viewing bias might be different from that in planar videos. The viewing bias in 360° videos might be more complex because users can get more content information with multiple viewpoints [14]. Besides, users start to watch 360° videos from the same viewing points no matter through VR head mounted devices or Youtube by PC, since the start-viewing point are fixed by 360 cameras. Nevertheless, currently, no visual saliency models possess the initial frame

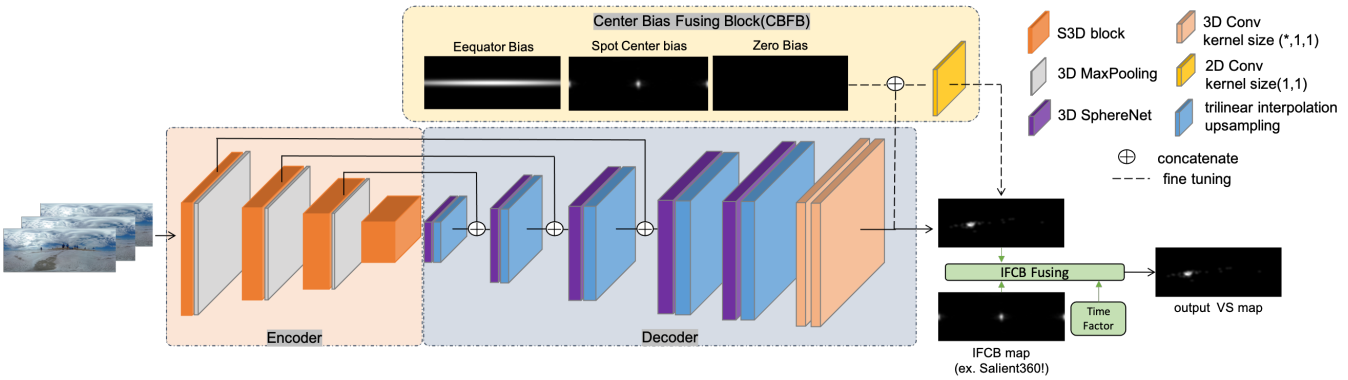

FIGURE 1. The overview of our model architecture. The encoder consists of S3D block, while the decoder is built with 3DSphereNet layers with trilinear interpolation upsampling layers. The last two layers of the decoder are 1×1 convolutional layers. The Center Bias Fusing Block fuses the three bias maps with the output of the decoder in pixel-wised manner by 1×1 convolution. Finally, the Initial Frame Center Bias(IFCB) module adds the IFCB map of a specific dataset and the time factor dependent on the frame number (see eq.2) to predict the final output VS map.

center bias effectively [8] which is an inevitable phenomenon of immersive videos as we have observed in the statistical data. The data type in 360° VS prediction can be separated into head movement (HM) and head+eye movement (HEM). The former determines the FoV regions seen by users when moving their heads, while the latter predicts users' eye gaze. We focus on HM saliency prediction in this paper since HM could be seen as the first step toward human attention [7].

In this paper, we proposed a 3D U-Net VS model with the combination of human viewing biases. Our model applies to equirectangular projection frames directly without any projection transformation. To cope with the oversampled polar regions in equirectangular frames, we introduced the 3D SphereNet specially desinged for 360° data and placed this module into the U-Net decoder. With the observation of the time-decay human viewing bias which is a special phenomenon in panorama videos, we proposed the inital frame center bias fusing methods, and analyzed the viewing biases between various 360° video VS datasets. Finally, with the aware of viewing bias observations, the Center Bias Fusing Block is proposed to fuse the well-founded viewing biases effectively. Empirical results on Salient360! [15], PVS [7] and Sport360 [6] datasets demonstrate the effectiveness of the proposed method.

The main contributions can be summarized as follows:

- With the observation of various initial viewing bias between datasets, we propose a learnable time-decay function to fuse the prediction map with different initial viewing bias effectively.
- We design center bias fusion block that improves the result of saliency prediction by considering the center bias statistics of different datasets and video categories.
- We extend SphereNet from 2D to 3D by applying the U-net model with 3D convolution and 3DSphereNet Decoder to deal with temporal data input.

II. RELATED WORK

A. VISUAL SALIENCY ON PLANAR VIDEOS

Most visual saliency (VS) prediction on videos have been done by deep convolutional neural networks. Different from VS prediction on images, temporal features are also considered in the VS video task. A majority of recent studies adopted recurrent neural networks to predict sequential fixation maps over successive frames. Wang et al. [13] applied attentive CNN-LSTM network to extract both static and dynamic saliency features. Wu et al. [16] extracted temporal information by a correlation-based ConvLSTM [17] which integrates the correlation information between frames. Droste et al. [18] made an unified model that predicts both images and videos with MobileNet and LSTM network.

Recently, 3D convolutional layers are also used in VS prediction tasks on planar videos. Some methods relied on the S3D architecture [19] which is a typical action detection backbone. Min et al. [10] was the first to introduce the S3D backbone into VS prediction task as the encoder that extracted spatial-temporal information. [9] used S3D bockbone as the U-Net encoder and added the auxiliary audio networks to predict audio-visual saliency.

Wang et al. [20] also adopted S3D backbone as the encoder backbone. For the decoder part, they applied self-attention mechanism to capture spatio-temporal information at multiple levels of the encoder. Further, considering the information gap between feature maps of different levels, they proposed AMSF module to integrate captured features from different levels.

Chang et al. [11] stacked feature pyramid network on top of the S3D encoder features and aggregated multi-scale feature maps to predict visual saliency. All these methods [9]–[11] achieved outstanding performance on planar video VS datasets, such as DHF1K [13]. While ConvLSTM [17] extracted temporal information only from the hidden state of the propagation from the succesive previous frames, 3D convolution [21] captured the temporal features encoded in multiple adjacent frames.

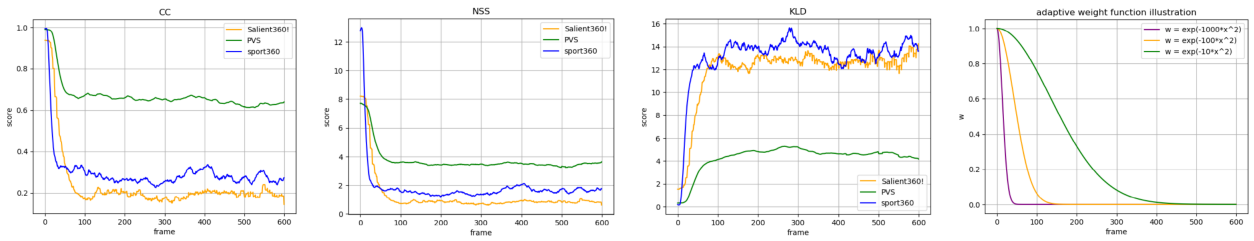

(a) (b) (c) (d)

FIGURE 2. (a), (b) and (c) are the CC, NSS, KLD score of IFCB map of the three datasets respectively. **??** is an illustration of equation 2. The slope of the curve becomes steeper as alpha increases..

B. VISUAL SALIENCY ON 360° VIDEOS

Some learning-based methods on 360° videos also emerged in the past three years. CubePadding [5] learned the model by weakly supervised learning with optical flow and video frames in the cubemap format. However, CubePadding was not suitable for static videos which do not have much optical flow features. Besides, CubePadding needed extra calculation to transform equirectangular frames into cube faces. SpherePHD [22] represents the spherical images on an icosahedron, and designs the convolution kernel under this representation. Spherical DNN [23] employs a circular crown kernel on the sphere instead of SphereNet using the traditional square kernel. Spherical U-Net [6] introduced a spherical convolution, involving the rotation of the crown kernel along the sphere, to tackle with the distortion of 360° videos in equirectangular frames. Spherical U-Net learned the model by teacher-forcing [24] that the ground-truth of previous frames were fed into the model during training and inferenced the result with previous predictions of the model, causing the performance degraded over time as the prediction becoming less accurate. DHP [7] proposed deep reinforcement learning (DRL) approach to predict head movement saliency map in an offline manner. They first transformed a specific subject's FoV regions into rectilinear projection and applied DRL prediction. However, during inference stage, DHP needed to run live fixation points of a specific user and later on collected several users' predicted fixation points to generate the saliency maps, which was inefficient. SPN [8] took optical flow and frames in the cubemap format as motion and spatial information and adopted Bi-ConvLSTM to extract temporal features. However, SPN needed extra computational costs on generating optical flow and the cubemap transformation. Although SPN considered human viewing bias by fusing different gaussian prior maps into feature maps by convolution layers, the gaussian prior maps used by SPN were chosen without the support of human viewing analysis in different datasets and video contents. In order to deal with initial viewing bias, SPN fused the average saliency map with optical flow motion features by element-wise product. However, this method ignored the time factor of initial frame viewing bias and the videos with less optical flow features, such as scenery videos.

III. METHOD

TABLE 1. The proportion of video categories in different datasets. *Miscellaneous* refers to videos that do not belong to the four main categories.

Dataset \ Video Type	Exploration	Static	Moving	Rides	Miscellaneous	Number of Video
Salient360!	42.10%	26.31%	15.78%	10.52%	5.26%	19
PVS	14.66%	12.00%	21.33%	28.00%	24.00%	75
Sport360	0.96%	2.88%	76.92%	19.23%	0.00%	104

TABLE 2. The CC score improvement of fusing each center bias maps in Fig.5.

Video type \ Prior maps	Fig.5 (a)	Fig.5 (b)	Fig.5 (c)	Fig.5 (d)
Exploration	5.52%	3.18%	2.10%	1.51%
Moving Focus	-1.78%	-0.40%	-0.27%	-0.46%
Static Focus	-1.05%	2.47%	4.46%	2.63%
Rides	12.95%	0.69%	0.27%	4.50%

A. NETWORK STRUCTURE

1) Spatial-Temporal Encoder.

The proposed model architecture is composed of an encoder followed by a decoder with multi-branch skip connections, as illustrated in Fig.1. The encoder is S3D network [19] extracting spatial-temporal features through 3D convolution and 3D maxpooling. We use S3D network since it replaces standard 3D convolution with the separable spatial and temporal convolutional blocks which encode the spatial-temporal information efficiently with lower computational costs. Moreover, the pre-trained weight of S3D network on the Kinetics dataset [25] which is a large action-recognition dataset is available, making it fast and effective for transfer-learning on the limited visual saliency data. Thus, we use the pre-trained S3D weight as the initial weight of the encoder. The input of the encoder is a sequence of T frames $\{I_{t-T+1}, ..., I_t\}$, where I_t is the equirectangular frame of the video at time t. Then the encoder extracts four scales of spatial-temporal feature maps: F_1, F_2, F_3, F_4 as the later input of the decoder, where F_1, F_2, F_3, F_4 are 1/4x, 1/8x, 1/16x, and 1/32x to the original input frames respectively.

2) 360 Kernel Decoder.

While the encoder contains standard convolutional kernel, the decoder consists of 3D SphereNet layers which are 3D

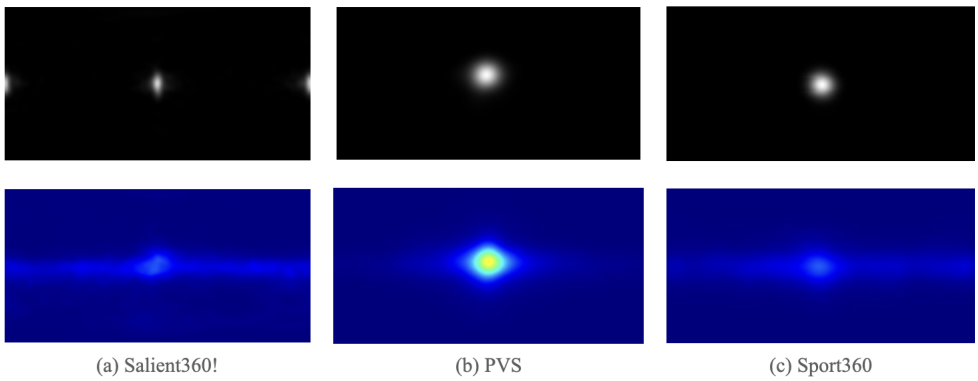

FIGURE 3. Top row: IFCB maps. Bottom row: Average saliency maps with frame number over 100.

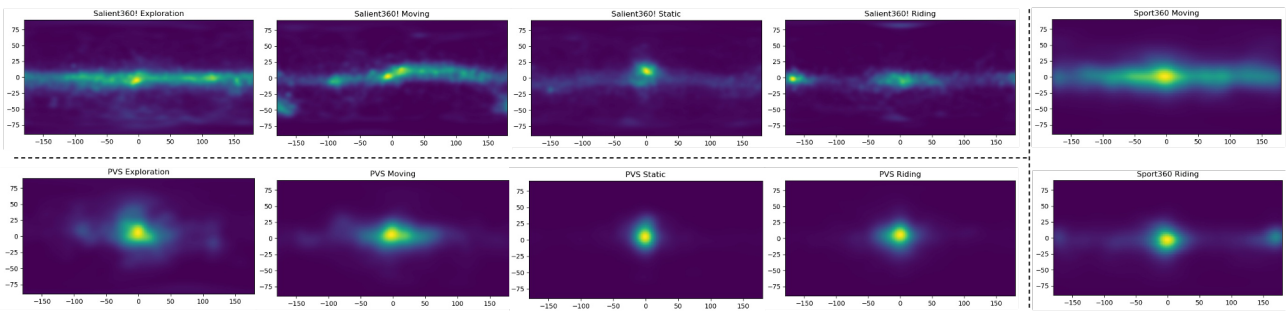

FIGURE 4. The averaged saliency maps (normalized to $[0, 1]$) with frame number over 100 of four main video catogries over various datasets. Note that we only illustrate salieny maps that are *Rides* and *Moving Focus* types in Sport360 since most of the videos within belong to these two categories, while the *Exploration* and *Static Focus* video types are too few to be of statistical significance.

kernels expanded from SphereNet [26] used in 360° image classification and object detection. Due to the oversampling around the polar regions in equirectangular projection, we adpot SphereNet kernels which are able to extract repeating features into our decoder module. SphereNet calculates the coordinates of input pixel of convolution by inverse gnomonic projection from the center of kernel. Besides, in order to avoid discontinuities in equirectangular projection, SphereNet automatically wraps the sampling points at the left and right boundaries. We extend SphereNet from 2D to 3D by applying the U-net model with 3D convolution and 3DSphereNet Decoder to deal with temporal data input. To extend SphereNet from 2D to 3D, we sample the input coordinates by an inverse gnomonic projection, which is adapted in SphereNet among spatial dimensions, and use trilinear interpolation [27] for sampling among temporal dimensions. The inputs of the decoder are F_1,F_2,F_3, and F_4. Except for F_1, the three feature maps: F_2, F_3, and F_4 are passed into the decoder using skip connection and concatenated with the feature maps. F_1 and the concatenated feature maps are decoded by 3D SphereNet layers and are upsampled by trilinear interpolation method. Finally, the decoder outputs a visual saliency prediction map of time t that corresponds to the last frame I_t of the encoder input sequence.

B. INITIAL FRAME CENTER BIAS

It is a common practice for users to start exploring the 360° videos in the same Field of View (FoV). In other words, users tend to watch the same portion of 360° frames, namely the same longitude and latitude coordinates, at the very beginning of 360 videos. In fact, this initial frame center bias is common in 360° visual saliency dataset, because the start-watching point is determined by the devices, such as 360 cameras. [8] considered the initial frame center bias by considering both center bias map and the motion features with residual mechanism. However, this method ignored the vanishing phenomenon of the initial center bias over time.

We designed the initial frame center bias (IFCB) fusing method based on our statistical findings over three datasets: Salient360! [15], PVS [7], Sport360 [6] with the CC, NSS, and KLD metrics; both the dataset descriptions and metric details can be found in Section Experiment. We compute the average of the first visual saliency frames from the training data of the three datasets, which we refer as IFCB map (the top row of Fig.3) and calculated its CC, NSS and KLD scores with ground-truth saliency maps. In Fig.2, the score of IFCB maps from three datasets are shown respectively. Obviously, in all datasets, the CC and NSS scores of IFCB maps are extremely high at the initial frames and gradually degrade as the time increases, which indicates that users spread their view from the same starting point and looked around independently. The low KLD scores at the initial

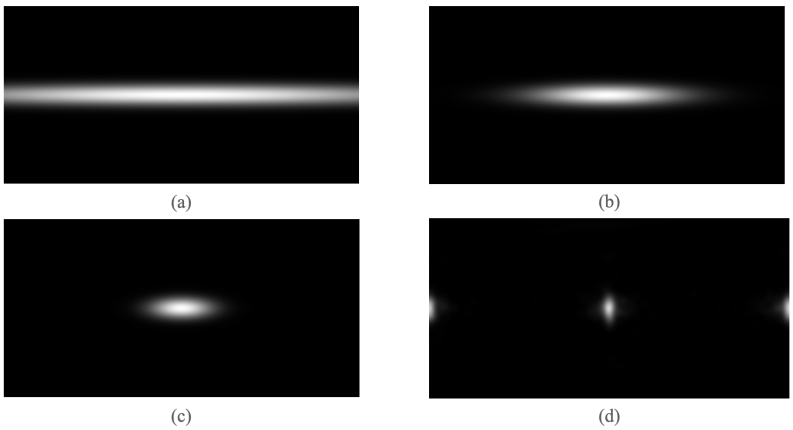

FIGURE 5. 5(a)- 5(c) are gaussian map generated by eq.3 with the same means: $\mu_x = \mu_y = 0.5$ and standard deviation: $(\sigma_x, \sigma_y) = (0.5, 0.02)$, $(\sigma_x, \sigma_y) = (0.15, 0.02)$, $(\sigma_x, \sigma_y) = (0.06, 0.02)$, respectively. 5(d) is the IFCB map of Salient360.

frames also imply that the probability distribution of IFCB map pixels is similar to that of the ground truth at the beginning. Therefore, adding IFCB maps and the time-decay factor into the prediction procedure should be beneficial.

The initial frame center bias of the three datasets are slightly different. In Salient360! dataset, the start-watching points are at longitude $0°$ or the opposite $180°$ (the top row of Fig.3(a). In PVS and Sport360 dataset, the users all start looking from longitude $0°$ with some latitude offsets (the top row of Fig.3(b) - 3(c). Furthermore, in Fig.2, the declining or rising rate of the evaluation scores various between datasets. For example, the CC score of the Sport360 IFCB map decreases drastically from score 1 to 0.4 within 50 frames. On the other hand, the CC score of PVS IFCB map reduces at a slower rate from score 1 to 0.7 within 100 frames. Considering the existing IFCB difference between datasets, we propose an adaptive weighting method to dynamically learn the fusing weights of IFCB map and the decoder prediction map with a time-decaying function. Here, for simplicity, we assume the weighted fusing mechanism is given as

$$P_t = w_t \times IFCB + (1 - w_t) \times D_t, \quad (1)$$

where D_t represents the output saliency map of the decoder at time t, and P_t is the final prediction saliency map as a linear combination of D_t and IFCB with adaptive weight w_t. Based on the observed time-dependence of the evaluated CC, NSS, KLD scores of IFCB to the ground-truth saliency maps (Fig.2(a) - 2(c)), we adopt a Gaussian decay function (Fig.2(d)) for the adaptive weight as follows:

$$w_t = \exp(-\alpha(t/C)^2), \quad (2)$$

where C is a constant which we set as 600 in our experiments. Instead of being fixed, α is automatically learned by fine-tuning the whole model. Here we frame the weight as a decay function. Because as the 360 video plays, according to our observation, the user's sight gradually spreads out from the center to varying extents in different video categories.

C. POTENTIAL CENTER BIAS

1) Center Bias Analysis

Human attention might have varying viewing bias when watching panoramic videos. In order to have a further observation on human viewing center bias, we analyze the ground-truth saliency maps of each dataset and different video categories and have the following findings. *Finding(1)*: Datasets exist distinct center bias. *Finding(2)*: Fusing different kinds of center bias improves the performance variously in four video categories.

First, we average the saliency maps with frame number over 100 of the three datasets as shown in the bottom row of Fig.3. From Fig.3, we can see that PVS has a strong center bias without a doubt. On the contrary, Salient360! has a little bias at the equator, and Sport360 has almost no center bias. This indicates that various datasets exist with different degrees and distributions of center viewing bias, which is our *Finding(1)*. Second, according to a study in [28] which shows that the Region of Interest (ROIs) that attracts human attention depends on the video content itself, we manually classify the videos of the three datasets into four categories (Table 1):

- *Exploration*: Users tend to explore the entire sphere since there is no particular object or moving direction in scenes, such as landscape.
- *Static Focus*: The salient objects are standstill at the frame center, such as music concert.
- *Moving Focus*: There are eye-catching objects moving over the sphere in the video, such as sport videos.
- *Rides*: Videos are shoot with camera fast moving forward to a specific direction, such as car driving videos.

We average and normalize the ground-truth saliency maps with frame number over 100 of each category, as illustrated in Fig.4. To observe the impact of various center biases on different video categories, we fuse four kinds of center bias maps in Fig.5 which have different coverage on the equator into our Salient360! prediction output with linear

combination. Note that the first to third center bias maps in Fig.5 (a)-(c) are generated by the equation as follows.

$$f(x,y) = \frac{1}{2\pi\sigma_x\sigma_y}\exp\left(-\frac{(x-\mu_x)^2}{2\sigma_x^2} - \frac{(y-\mu_y)^2}{2\sigma_y^2}\right) \quad (3)$$

The means μ_x and μ_y both equal to 0.5 in the first to third center bias maps Fig.5 (a)-(c); the standard deviations are $\sigma_y = 0.02$ and $\sigma_x = 0.5, 0.15, 0.06$, respectively. The fourth center bias map 5 (d) is the IFCB map of Salient360!. In Table 2, by fusing the aforementioned four kinds of center bias maps, the CC scores are improved in different degrees depending on the video category. It appears that the *Moving Focus* video type does not benefit from the center bias. This may be because the eye-catching moving objects appear irregularly in various places near the equator. As for the *Exploration* category, the improvement grows as the coverage on the equator becomes larger in center bias map. Since *Exploration* type videos lack salient objects, users attention spread along the equator instead of focusing on the same point. The *Static Focus* video type consists of an obvious object in the frame center, so it benefits the most from the center spot bias (Fig.3 (c)). Finally, we observe that the *Rides* category videos benefit the most from center bias map that has little dependency on the longitude. Since users tend to watch in the direction of the camera motions, which happen to be at longitude $180°$ in videos that we test in Table 2, the center biases as depicted in 5 (a) and 5 (d), having values on the $180°$ longitude region, make the more improvement.

2) Learned Center Bias Fusing

Through the two findings in Section.III-C-Center Bias Analysis, we have a better understanding of the viewing bias in three datasets:

1) Sport360: The video category classification results in Table 1 shows that videos in Sport360 mostly belong to the *Moving Focus* type, which implies that sport360 exhibits nearly no center bias, supported by our *Finding(2)*.
2) PVS: Compared with the other two datasets, the proportion of each video category in PVS is relatively average (Table 1), but the viewing biases have few differences in the four video categories (Fig.5). Obviously, PVS itself exists strong center bias in all video categories, supported by our *Finding(1)*.
3) Salient360!: Different from PVS, Salient360! has a little bias at the equator according to our *Finding(1)*. Besides, there are up to 40% videos belong to *Exploration* type in Salient360! which benefit more from equator center bias. Thus, the equator viewing bias existing in Salient360! can also be partially explained by our *Finding(2)*.

According to the understanding that we conclude above, it is necessary to manage the different extents of center bias among datasets. Through the analysis of composition of the three datasets (Table 1), PVS composes more of spot center bias, while Salient360! consists more of equator bias. On the other hand, Sport360! contains nearly no viewing bias. Thus, We introduce Center Bias Fusing Block(CBFB) (Fig. 1). In CBFB, we concatenate equator bias map 5(a), the spot center bias, zero bias map denoting no bias, and the output map of the decoder (Fig.1). Note that we use IFCB map as the spot center bias map since the initial watching regions set by the camera devices are also the center regions of the video. We then pass the concatenation map into an one-by-one convolution, learning the fusing weight by weighted sum. The CBFB module learn the fusing weights of different viewing biases from the given training data. Finally, the whole model is trained with IFCB and CBFB.

IV. EXPERIMENT

A. DATASET

- Salient360!: The dataset Salient360! [15] is a benchmark carried out by Salient360! Grand Chanllenges at ICME'17 and ICME'18 for 360° image and video saliency prediction. The benchmark provides 19 equirectangular 360° videos each lasting 20 seconds with head movement saliency maps recorded from 57 subjects [29].
- PVS: PVS dataset [7] includes 75 omnidirectional videos each lasting 10 to 80 seconds with head movement saliency maps recorded from 58 subjects. The video contents are diverse, including animation, driving, sports, movies and scenery. The author of PVS splits the data into 60 training videos and 15 testing videos.
- Sport360: The videos of Sport360 are from [30] with the head movement saliency maps collected by [6]. Sport360 contains 104 360° sport videos, such as basketball, skateboarding and parkour, with the duration of 20 to 60 seconds viewed by 20+ subjects. Following the settings in [6], we use 80 video sequences for training, and 24 video sequences for testing.

B. IMPLEMENTATION DETAIL

1) Loss Function

Our saliency prediction model is trained by minimizing an integration of several well adopted evaluation metrics. Here we take the combination of *Kullback-Leiber divergence*(KLD), *Pearson's Correlation Coefficient(CC)* and *Normalized Scanpath Saliency (NSS)* metrics as our loss function in the following expression:

$$\begin{aligned} L(P, Q^d, Q^f) = &\lambda_{KL} KL(P, Q^d) - \\ &\lambda_{CC} CC(P, Q^d) - \\ &\lambda_{NSS} NSS(P, Q^f), \end{aligned} \quad (4)$$

where we take $\lambda_{KL} = 2$, $\lambda_{CC} = 0.8$, $\lambda_{NSS} = 0.05$ empirically. The notations are given below:

- P: The predicted saliency map.
- Q^f: The binary fixation ground-truth map that refer to the original fixation locations.

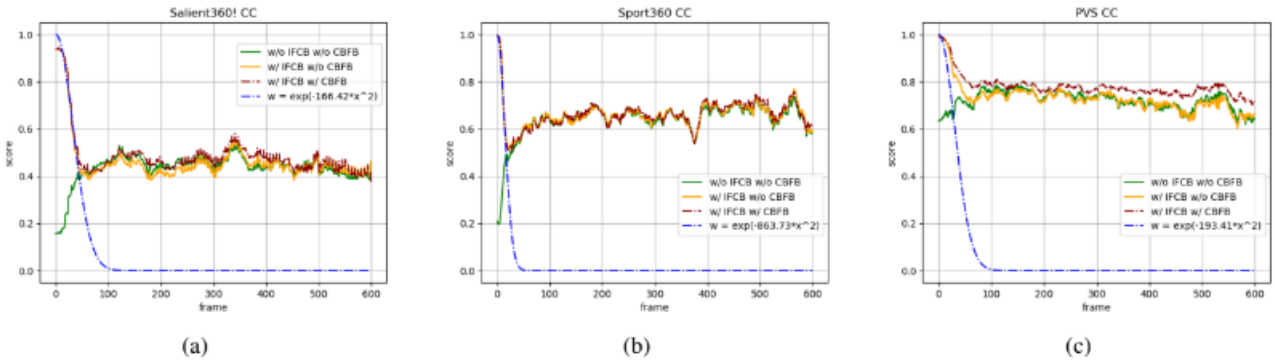

FIGURE 6. (a), (b), and (c) are the CC score of Salient360!, Sport360 and PVS with and without the IFCB module and CBFB module. The final result of IFCB fusing weights were also shown.

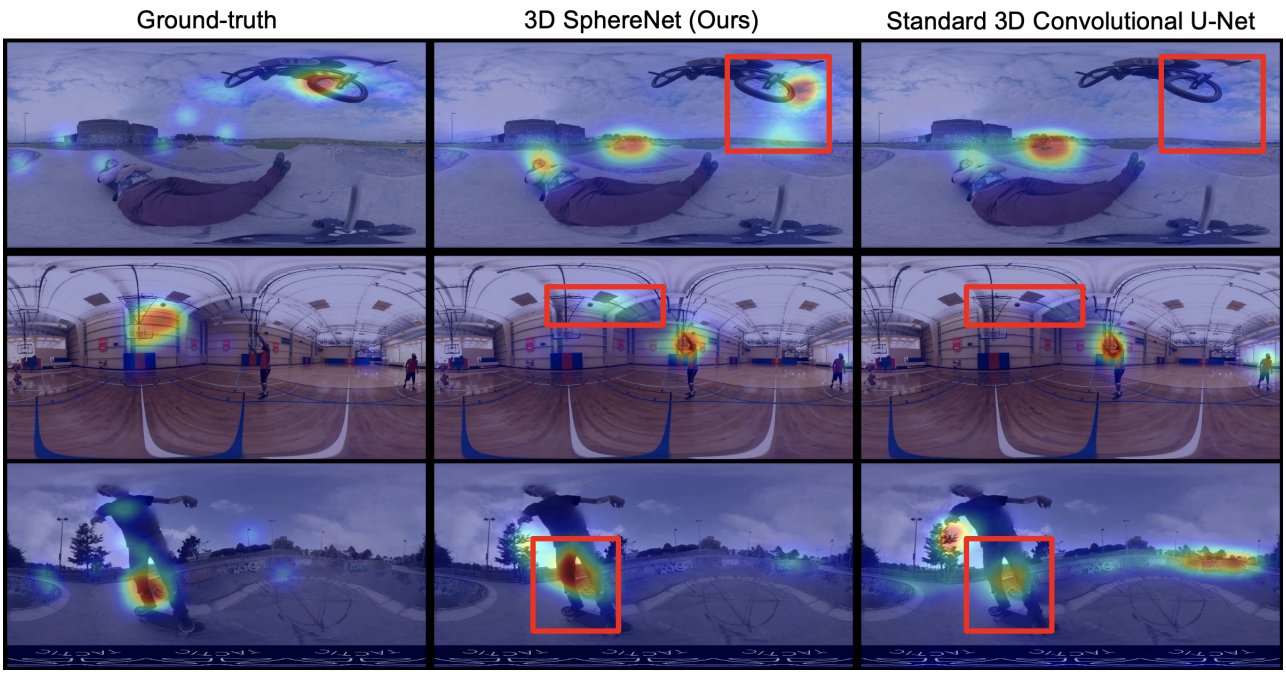

FIGURE 7. The saliency map visualization of the ground-truth(left), our 3D SphereNet (middle), and the standard 3D convolutional U-Net (right).

- Q^d: The density distribution ground-truth map that is smoothed by the Gaussian kernel on Q^f [31].
- The NSS metric is specially designed for saliency maps [32] and is defined as

$$NSS(P, Q^f) = \frac{1}{N} \sum_i \bar{P}_i \times Q_i^f, \tag{5}$$

where i refers to the i^{th} pixel in Q^f and P respectively. $N = \sum_i Q^f$, and $\bar{P} = \frac{P - \mu(P)}{\sigma(P)}$ where μ and σ are mean and standard deviation of P.

- The CC metric measures the correlation between two distributions as

$$CC(P, Q^d) = \frac{cov(P, Q^d)}{\sigma(P) \times \sigma(Q^d)}, \tag{6}$$

where $cov(P, Q^d)$ stands for the covariance of P and Q^d, and $\sigma(\cdot)$ denotes the corresponding standard deviation.

- The KLD measures the dissimilarity between predicted saliency and ground-truth distribution which is defined as

$$KL(P, Q^d) = \sum_i Q_i^d \log \left(\epsilon + \frac{Q_i^d}{\epsilon + P_i} \right), \tag{7}$$

where ϵ is a regularization constant.

2) Training and Testing

Our implementation is on top of PyTorch framework [33]. The model is trained in two stages. First, we train the encoder initialized with weights pre-trained on the Kinetics dataset [25], and the decoder from scratch until they converge. Then we train the full model in the second stage, including CBFB and IFCB. The Adam optimizer is used with the learning

rate 1×10^{-4} at the first stage and 1×10^{-5} at the second stage. The input sequence length is 32 and in equirectangular format without any projection transformation with batch size 4. All frames are resized to 224×384. For Salient360! dataset, we split the data into 15 videos for training and 4 for validation. As for PVS dataset, we randomly split the training data into 50 training videos and 10 validation videos. When training on Sport360 dataset, we choose 10 videos randomly as validation data, and the rest 70 videos as training data. We evaluate our model on the testing videos used in DHP [7] and Spherical-Unet [6] of PVS dataset and Sport360 dataset respectively. As for Salient360!, since the ground-truth of the testing data is not available, we evaluate our model on the validatation set.

3) Evaluation Metric

In addition to evaluating our method with KLD, CC and NSS metrics, we also consider *Similarity*(SIM), AUC-Judd and shuffled-AUC metrics [34]. The details of these metrics can be found in [31].

In view of the heavy distortion near the pole regions under equirectangular projections, the Salient360! benchmark corrected the oversampled pole areas by applying a latitudinal sinusoidal factor [29] to the saliency maps during evaluation. Here we also report the results adjusted by the latitudinal sinusoidal factors with asterisk symbol ($*$).

C. EXPERIMENTAL RESULT

1) Ablation Study

We perform ablation studies to evaluate the contribution of each component of the proposed network. In Table 3, we compare our modules with standard 3D convolution U-Net. All the components, including 3DSphereNet decoder, IFCB, and CBFB improve the performance in some extent. The 3D SphereNet decoder enhances most of the evaluation metric score except for the KLD/AUC-Judd score in PVS and the CC/NSS score in Sport360. With the combination of 3D SphereNet decoder and IFCB module, the CC score improved about 3.1% on Salient360!, 1.34% on PVS and 1.76% on Sport360. Besides, from Fig.6, the CC scores of the initial frames are raised with the IFCB module. As for CBFB module, the CC scores increase 2.31% on Salient360!, 4.73% on PVS, and 0.36% on Sport360. The different magnitudes of the progress between the three datasets correspond to our first finding that different datasets exhibit distinct degrees of center bias (Section.III-C-Center Bias Analysis).

2) Quantitative Result

We compare our model with state-of-the-art 360° video visual saliency models including ViNet [9] dealing with planar video, STSANet [20], Spherical U-Net [6], DHP [7], SPN [8], V-BMS [35], MT-DNN [36] and Spherical DNN [23]. In order to show the effectiveness of IFCB fusing by eq.1, we used IFCB maps directly as our baseline. Our model beats the baseline in all three datasets. Table.4, Table.5 and Table. 6 show the quantitative results of the different methods.

TABLE 3. The ablation study on the effectiveness of various modules in the proposed model. Standard-3DUnet refers to the U-net model with 3D Convolution, and 3DSphereNet is the 3DUnet with our 3DSphereNet Decoder.

Salient360!					
Method \ Metrics	CC↑	NSS↑	KLD↓	SIM↑	AUC-J↑
Standard-3DUnet*	0.3998	1.7924	6.6621	0.3212	0.8749
3DSphereNet*	0.4336	1.9402	6.4355	0.3325	0.8852
3DSphereNet* w/ IFCB	0.4645	2.2537	5.9410	0.3599	0.8891
3DSphereNet* w/ IFCB w/ CBFB	**0.4877**	**2.3502**	**5.7021**	**0.3759**	**0.8927**
PVS					
Method \ Metrics	CC↑	NSS↑	KLD↓	SIM↑	AUC-J↑
Standard-3DUnet*	0.6863	3.3031	3.8697	0.5115	0.9280
3DSphereNet*	0.7069	3.3820	3.8869	0.5184	0.9272
3DSphereNet* w/ IFCB	0.7203	3.5330	3.4999	0.5395	0.9295
3DSphereNet* w/ IFCB w/ CBFB	**0.7676**	**3.7498**	**3.2084**	**0.5661**	**0.9325**
Sport360					
Method \ Metrics	CC↑	NSS↑	KLD↓	SIM↑	AUC-J↑
Standard-3DUnet*	0.6482	4.4184	5.3503	0.4605	0.9360
3DSphereNet*	0.6449	4.3638	5.0717	0.4654	0.9370
3DSphereNet* w/ IFCB	0.6625	4.5393	**4.8101**	0.4790	0.9375
3DSphereNet* w/ IFCB w/ CBFB	**0.6661**	**4.5860**	4.8529	**0.4793**	**0.9402**

TABLE 4. The comparison on the testing data of PVS, where the asterisk symbol ($*$) represents the results adjusted by the latitudinal sinusoidal factors and the dagger symbol (†) represents the reproduced testing result, otherwise it is testing result reported by original paper.

Method \ Metrics	CC↑	NSS↑	sAUC↑
baseline†	0.633	3.243	0.519
ViNet†	0.633	2.447	0.643
STSANet†	0.743	3.538	0.806
STSANet w/IFCB w/CBFB†	0.6	2.827	0.799
DHP	0.704	3.275	0.700
Spherical U-Net†	0.745	3.175	0.700
MT-DNN	0.675	3.115	\
SPN*†	0.767	3.289	0.752
SPN* w/IFCB w/CBFB †	**0.783**	3.607	0.792
3DSphereNet†	0.7069	3.382	\
3DSphereNet w/IFCB w/CBFB†	0.757±0.005	**3.768±0.029**	**0.820±0.004**
3DSphereNet* w/IFCB w/CBFB†	0.768±0.005	3.760±0.031	0.818±0.004

We had added initial frame center bias (IFCB) and Center Bias Fusing Block (CBFB) to SPN and STSANet. SPN is the current state-of-the-art saliency prediction model proposed on 360 videos, and STSANet is proposed on the planar video. The experimental results provided in Table.4, Table. 5 and Table. 6 show that adopting IFCB and CBFB to SPN and 3DSphereNet enhances the evaluation metric score compare to our reproduced results. However, adopting IFCB and CBFB to STSANet does not as good as the proposed model. We presume that our proposed IFCB and CBFB can be applicable to the model designed for 360 videos. On the other hand, We reproduced SPN model according to SPN paper description to the best of our knowledge. However, the reproduced results do not meet those reported by [8] (see supplementary materials for more details). Due to the absence of testing ground-truth of Salient360!, we only compare with ViNet and DHP which are reproducible with their open source code on the validation set (Table 6). We also upload the testing result of Salient360! onto the benchmark website, and achieve the best results (Table 6) on CC, NSS, KLD, SIM metrics. [1]

[1]https://mmcheng.net/videosal/

TABLE 5. The comparison on the testing data of Sport360.

Method \ Metrics	CC↑	NSS↑	AUC-J↑
baseline†	0.1761	1.0931	0.2535
ViNet†	0.6320	4.3845	0.9244
STSANet†	**0.682**	4.316	0.906
STSANet w/IFCB w/CBFB†	0.624	3.665	0.894
DHP†	0.4445	2.5913	0.8744
Spherical U-Net	0.6246	3.5340	0.8977
SPN*†	0.4377	3.9351	0.931
SPN* w/IFCB w/CBFB†	0.6054	**4.9311**	**0.9425**
3DSphereNet*†	0.6449	4.3638	0.9370
3DSphereNet w/IFCB w/CBFB†	0.6627±0.003	4.5804±0.039	0.9299±0.002
3DSphereNet* w/IFCB w/CBFB†	0.6668±0.003	4.5674±0.039	0.9399±0.001

TABLE 6. The comparison on the validation data of Salient360!. The last row is our model result on the testing data of the Salient360! benchmark.

Method \ Metrics	CC↑	NSS↑	KLD↓	SIM↑	AUC-J↑
baseline†	0.216	1.130	12.768	0.198	0.402
ViNet†	0.400	1.846	6.694	0.314	0.873
STSANet†	0.354	1.578	**1.889**	0.297	0.851
STSANet w/IFCB w/CBFB†	0.257	1.203	2.436	0.25	0.757
DHP†	0.175	1.052	15.453	0.2007	0.474
V-BMS	0.383	1.614	4.995	—	0.815
Spherical DNNs	0.4087	0.6989	—	—	0.6594
3DSphereNet*†	0.4336	1.9402	6.4355	0.3325	0.8852
3DSphereNet* w/IFCB w/CBFB†	**0.483±0.004**	**2.315±0.030**	5.850±0.113	**0.369±0.005**	**0.892±0.001**
3DSphereNet* w/IFCB w/CBFB† (Testing)	0.471	2.087	3.044	0.432	0.817

3) Qualitative Result

We compare our model with the standard 3D convolutional U-Net using the visualization result of the saliency map, as demonstrated in Fig. 7. In Fig. 7, standard 3D convolution fails to detect distorted salient areas nearby polar regions, such as the flying bike's wheel or the flying basketball. Moreover, the 3D convolution will pay more attention to the salient object on the equator instead of the distorted legs on the skateboard in the third row of Fig.7. By applying 3D SphereNet, the model can detect salient distorted areas that appear in the panorama.

V. DISCUSSION

In this section, we point out future works and the limitations of our model. The limitations of our model are listed below:

1) There are few 360° visual saliency datasets and benchmarks, we could only train our model on the currently existing three datasets, which are also used in the previous works. We are willing to apply our proposed model to other types of videos when such datasets are available.
2) The inference speed of the proposed model is not fast enough to apply to real-time visual saliency prediction, which is also a critical issue in the practical application.

Unlike previous works focusing on planar (2D) videos, we focus on 360 (3D) videos. The immersive experience brought by 360 videos allows the users to have various viewing angles to watch, which causes the viewing bias that does not exist in planar videos. The viewing bias is a special viewing phenomenon in 360 videos; therefore, it is important to face up to the viewing bias issue and improve our 360 model. We list several future works as follows:

1) Collect more videos to further verify our model's generalization ability and the proposed viewing bias method.
2) Further adjust the architecture of the proposed model to make it more lightweight for practical applications.

VI. CONCLUSION

In this paper, we address the special phenomenon caused by initial frame viewing bias existing in 360° videos using learnable time-decaying curves, coping with the various time-decay rates among datasets. It is to our observation that datasets need various viewing biases based on the analysis of saliency maps across different datasets, video types and the improvements using multiple center bias maps. Thus, the proposed center bias fusing block learned to find the proper weights of different bias maps of each datasets. We utilize 3D convolution to a spatial-temporal encoder and propose 3D SphereNet ketnerls for the decoder in order to deal with the oversampling of feature maps in polar regions. The proposed method achieve the state-of-the-art results on three publicly available 360° visual saliency datasets, including Salience360!, PVS, and Sport360.

REFERENCES

[1] Filip Škola, Selma Rizvić, Marco Cozza, Loris Barbieri, Fabio Bruno, Dimitrios Skarlatos, and Fotis Liarokapis, "Virtual reality with 360-video storytelling in cultural heritage: Study of presence, engagement, and immersion," Sensors, vol. 20, no. 20, pp. 5851, 2020.

[2] Jaziar Radianti, Tim A Majchrzak, Jennifer Fromm, and Isabell Wohlgenannt, "A systematic review of immersive virtual reality applications for higher education: Design elements, lessons learned, and research agenda," Computers & Education, vol. 147, pp. 103778, 2020.

[3] Hyunae Lee, Timothy Hyungsoo Jung, M Claudia tom Dieck, and Namho Chung, "Experiencing immersive virtual reality in museums," Information & management, vol. 57, no. 5, pp. 103229, 2020.

[4] Ulrich Neumann, Thomas Pintaric, and Albert Rizzo, "Immersive panoramic video," in Proceedings of the eighth ACM international conference on Multimedia, 2000, pp. 493–494.

[5] Hsien-Tzu Cheng, Chun-Hung Chao, Jin-Dong Dong, Hao-Kai Wen, Tyng-Luh Liu, and Min Sun, "Cube padding for weakly-supervised saliency prediction in 360 videos," in Proceedings of the IEEE Conference on Computer Vision and Pattern Recognition, 2018, pp. 1420–1429.

[6] Ziheng Zhang, Yanyu Xu, Jingyi Yu, and Shenghua Gao, "Saliency detection in 360 videos," in Proceedings of the European conference on computer vision (ECCV), 2018, pp. 488–503.

[7] Mai Xu, Yuhang Song, Jianyi Wang, MingLang Qiao, Liangyu Huo, and Zulin Wang, "Predicting head movement in panoramic video: A deep reinforcement learning approach," IEEE transactions on pattern analysis and machine intelligence, vol. 41, no. 11, pp. 2693–2708, 2018.

[8] Youqiang Zhang, Feng Dai, Yike Ma, Hongliang Li, Qiang Zhao, and Yongdong Zhang, "Saliency prediction network for 360° videos," IEEE Journal of Selected Topics in Signal Processing, vol. 14, no. 1, pp. 27–37, 2019.

[9] Samyak Jain, Pradeep Yarlagadda, Shreyank Jyoti, Shyamgopal Karthik, Ramanathan Subramanian, and Vineet Gandhi, "Vinet: Pushing the limits of visual modality for audio-visual saliency prediction," arXiv preprint arXiv:2012.06170, 2020.

[10] Kyle Min and Jason J Corso, "Tased-net: Temporally-aggregating spatial encoder-decoder network for video saliency detection," in Proceedings of the IEEE/CVF International Conference on Computer Vision, 2019, pp. 2394–2403.

[11] Qinyao Chang, Shiping Zhu, and Lanyun Zhu, "Temporal-spatial feature pyramid for video saliency detection," arXiv preprint arXiv:2105.04213, 2021.

[12] Marcella Cornia, Lorenzo Baraldi, Giuseppe Serra, and Rita Cucchiara, "Predicting human eye fixations via an lstm-based saliency attentive model," IEEE Transactions on Image Processing, vol. 27, no. 10, pp. 5142–5154, 2018.

[13] Wenguan Wang, Jianbing Shen, Fang Guo, Ming-Ming Cheng, and Ali Borji, "Revisiting video saliency: A large-scale benchmark and a new model," in Proceedings of the IEEE Conference on Computer Vision and Pattern Recognition, 2018, pp. 4894–4903.

[14] Shmuel Peleg and Moshe Ben-Ezra, "Stereo panorama with a single camera," in Proceedings. 1999 IEEE Computer Society Conference on Computer Vision and Pattern Recognition (Cat. No PR00149). IEEE, 1999, vol. 1, pp. 395–401.

[15] Erwan J David, Jesús Gutiérrez, Antoine Coutrot, Matthieu Perreira Da Silva, and Patrick Le Callet, "A dataset of head and eye movements for 360 videos," in Proceedings of the 9th ACM Multimedia Systems Conference, 2018, pp. 432–437.

[16] Xinyi Wu, Zhenyao Wu, Jinglin Zhang, Lili Ju, and Song Wang, "Salsac: A video saliency prediction model with shuffled attentions and correlation-based convlstm," in Proceedings of the AAAI Conference on Artificial Intelligence, 2020, vol. 34, pp. 12410–12417.

[17] SHI Xingjian, Zhourong Chen, Hao Wang, Dit-Yan Yeung, Wai-Kin Wong, and Wang-chun Woo, "Convolutional lstm network: A machine learning approach for precipitation nowcasting," in Advances in neural information processing systems, 2015, pp. 802–810.

[18] Richard Droste, Jianbo Jiao, and J Alison Noble, "Unified image and video saliency modeling," in European Conference on Computer Vision. Springer, 2020, pp. 419–435.

[19] Saining Xie, Chen Sun, Jonathan Huang, Zhuowen Tu, and Kevin Murphy, "Rethinking spatiotemporal feature learning: Speed-accuracy trade-offs in video classification," in Proceedings of the European conference on computer vision (ECCV), 2018, pp. 305–321.

[20] Ziqiang Wang, Zhi Liu, Gongyang Li, Yang Wang, Tianhong Zhang, Lihua Xu, and Jijun Wang, "Spatio-temporal self-attention network for video saliency prediction," IEEE Transactions on Multimedia, 2021.

[21] Shuiwang Ji, Wei Xu, Ming Yang, and Kai Yu, "3d convolutional neural networks for human action recognition," IEEE transactions on pattern analysis and machine intelligence, vol. 35, no. 1, pp. 221–231, 2012.

[22] Yeonkun Lee, Jaeseok Jeong, Jongseob Yun, Wonjune Cho, and Kuk-Jin Yoon, "Spherephd: Applying cnns on a spherical polyhedron representation of 360deg images," in Proceedings of the IEEE/CVF Conference on Computer Vision and Pattern Recognition, 2019, pp. 9181–9189.

[23] Yanyu Xu, Ziheng Zhang, and Shenghua Gao, "Spherical dnns and their applications in 360 images and videos," IEEE Transactions on Pattern Analysis and Machine Intelligence, vol. 44, no. 10, pp. 7235–7252, 2021.

[24] Ronald J Williams and David Zipser, "A learning algorithm for continually running fully recurrent neural networks," Neural computation, vol. 1, no. 2, pp. 270–280, 1989.

[25] Will Kay, Joao Carreira, Karen Simonyan, Brian Zhang, Chloe Hillier, Sudheendra Vijayanarasimhan, Fabio Viola, Tim Green, Trevor Back, Paul Natsev, et al., "The kinetics human action video dataset," arXiv preprint arXiv:1705.06950, 2017.

[26] Benjamin Coors, Alexandru Paul Condurache, and Andreas Geiger, "Spherenet: Learning spherical representations for detection and classification in omnidirectional images," in Proceedings of the European Conference on Computer Vision (ECCV), 2018, pp. 518–533.

[27] Ying Bai and Dali Wang, "On the comparison of trilinear, cubic spline, and fuzzy interpolation methods in the high-accuracy measurements," IEEE Transactions on fuzzy Systems, vol. 18, no. 5, pp. 1016–1022, 2010.

[28] Mathias Almquist, Viktor Almquist, Vengatanathan Krishnamoorthi, Niklas Carlsson, and Derek Eager, The Prefetch Aggressiveness Tradeoff in 360° Video Streaming, p. 258–269, Association for Computing Machinery, New York, NY, USA, 2018.

[29] Erwan J David, Jesús Gutiérrez, Antoine Coutrot, Matthieu Perreira Da Silva, and Patrick Le Callet, "A dataset of head and eye movements for 360 videos," in Proceedings of the 9th ACM Multimedia Systems Conference, 2018, pp. 432–437.

[30] Hou-Ning Hu, Yen-Chen Lin, Ming-Yu Liu, Hsien-Tzu Cheng, Yung-Ju Chang, and Min Sun, "Deep 360 pilot: Learning a deep agent for piloting through 360 sports videos," in 2017 IEEE Conference on Computer Vision and Pattern Recognition (CVPR). IEEE, 2017, pp. 1396–1405.

[31] Zoya Bylinskii, Tilke Judd, Aude Oliva, Antonio Torralba, and Frédo Durand, "What do different evaluation metrics tell us about saliency models?," IEEE transactions on pattern analysis and machine intelligence, vol. 41, no. 3, pp. 740–757, 2018.

[32] Robert J Peters, Asha Iyer, Laurent Itti, and Christof Koch, "Components of bottom-up gaze allocation in natural images," Vision research, vol. 45, no. 18, pp. 2397–2416, 2005.

[33] Adam Paszke, Sam Gross, Soumith Chintala, Gregory Chanan, Edward Yang, Zachary DeVito, Zeming Lin, Alban Desmaison, Luca Antiga, and Adam Lerer, "Automatic differentiation in pytorch," 2017.

[34] Ali Borji, Hamed R Tavakoli, Dicky N Sihite, and Laurent Itti, "Analysis of scores, datasets, and models in visual saliency prediction," in Proceedings of the IEEE international conference on computer vision, 2013, pp. 921–928.

[35] Pierre Lebreton, Stephan Fremerey, and Alexander Raake, "V-bms360: A video extention to the bms360 image saliency model," in 2018 IEEE International Conference on Multimedia & Expo Workshops (ICMEW). IEEE, 2018, pp. 1–4.

[36] Minglang Qiao, Mai Xu, Zulin Wang, and Ali Borji, "Viewport-dependent saliency prediction in 360 video," IEEE Transactions on Multimedia, vol. 23, pp. 748–760, 2020.

PENG-WEN CHEN received her B.S. degree in Engineering Science from National Cheng Kung University in 2019 and M.S. degree in Communication Engineering from National Taiwan University in 2021. Her research interests include both Computer Vision and Deep Learning. She currently works in MediaTek as Deep Learning Engineer and is responsible to optimize pre-silicon IR simulation flow by AI and computer vision algorithm.

TSUNG-SHAN YANG received his B.S. degree in both Chemistry and Electrical Engineering from National Taiwan University in 2019 and M.S. degree in Electrical Engineering from National Taiwan University in 2021. He is currently a Ph.D. student in Electrical Engineering at the University of Southern California. His research interests include machine learning and computer vision.

GI-LUEN HUANG was born in New Taipei, Taiwan. He received a B.S. degree in electrical engineering (EE) from the National Taiwan University of Science and Technology (NTUST), in 2021. He is currently a master's degree student at National Taiwan University (NTU) in Taipei, Taiwan. His research interests include computer vision, deep learning, and signal processing. He was nominated for the best student paper award at International Conference on System Science and Engineering (ICSSE), in 2020. He was a machine learning engineer intern at Jubo Tech. in New Taipei, Taiwan.

CHIA-WEN HUANG received her B.S. degree in Information Management from National Taiwan University in 2022. She is currently a master's degree student in the Data Science and Smart Network group of Communication Engineering at National Taiwan University. Her research interests include Deep Learning and Computer Vision.

YU-CHIEH CHAO received his B.S. degree in Computer Science and Information Engineering from National Central University in 2020 and M.S. degree in Communication Engineering from National Taiwan University in 2022. He is currently a Research Assistant at Academia Sinica. His research interests include Machine Learning, Deep Learning, Computer Vision, and Natural Language Processing.

CHIEN-HUNG LU has been the founder and CEO at Unusly in San Francisco since 2020. He earned a Ph.D. in electrical engineering from Princeton University in 2015, then worked in the industry as an optical scientist at Google from 2015 to 2019. He was the winner of Emil Wolf Outstanding Paper Competition in 2014.

PEI-YUAN WU is an assistant professor at NTUEE since 2017. He was born in Taipei, Taiwan, R.O.C., in 1987. He received the B.S.E. degree in NTUEE in 2009, and the M.A. and Ph.D. degree in Electrical Engineering from Princeton University in 2012 and 2015, respectively. Dr. Wu has joined TSMC from 2015 to 2017. He was a recipient of the Gordon Y.S. Wu Fellowship in 2010, Outstanding Teaching Assistant Award at Princeton University in 2012, as well as 2020 FutureTech Breakthrough Award held by MOST. His research interest lies in artificial intelligence, signal processing, estimation and prediction, and cyber-physical system modeling.